Mon. Not. R. astr. Soc. (1976) **177**, 485–497.

OPTIMUM DESIGN OF A CODED MASK X-RAY TELESCOPE FOR ROCKET APPLICATIONS

J. Gunson

Department of Mathematical Physics, University of Birmingham, Edgbaston, Birmingham

*and B. Polychronopulos**

Department of Space Research, University of Birmingham, Edgbaston, Birmingham

(Received 1976 July 12; in original form 1975 March 12)

SUMMARY

A review of the principles of current X-ray telescopes is made with particular emphasis on two-step imaging techniques involving coding masks. The merits and limitations of the various types of coding masks in use are examined in detail. The limitations are shown to arise from the finite nature of practical masks. By postulating periodicity, 'optimum masks' can be constructed with ideal imaging qualities. The theory for the design of such masks and the practical considerations involved in the design of a rocket-borne X-ray telescope system are discussed in full, with particular attention paid to resolution, field of view and image noise. The main emphasis throughout the paper is on one-dimensional masks but two-dimensional masks are also studied. It is concluded that optimum masks could prove very valuable in astronomical applications and also in other fields such as radiography, where high imaging quality coupled with high sensitivity and low cost are of utmost importance.

1. INTRODUCTION

X-ray astronomy using rocket, satellite or balloon-borne telescopes requires light, compact instruments of high resolution and effective aperture. Telescopes based on grazing incidence mirrors tend to have unfavourable aperture/mass ratio. Those based on mechanical or rotational collimators (**1**) have low resolving power and/or poor imaging properties. In this paper we consider a third type of instrument, based on a two-step imaging technique which can combine high resolution with large aperture/mass ratio and simplicity of construction.

This two-step technique, first suggested by Mertz (**2**) involves the formation of a shadowgram of the X-ray source by means of a coded shadow mask built up from opaque and transparent elements. The shadowgram is recorded on a suitable position-sensitive detector. The recording is then processed in the laboratory to reconstruct the desired image of the X-ray source.

Let f, g and h be respectively the source image function, the shadowgram function and the mask point source response function. Ray optics gives the basic convolution relation

$$g(\xi) = (f*h)/(\xi) = \int_{-\infty}^{+\infty} f(x)\, h(\xi - x)\, dx \qquad (1)$$

* Present address: BAC Ltd, Filton, Bristol.

in the case of one-dimensional imaging. If the convolution of h with itself is the Dirac δ-function, then the desired image function f is simply obtained by convoluting g with h. In other words, the autocorrelation function of the mask point source response function must possess a single sharp peak. Known examples of masks exhibiting this property are the Fresnel mask and the random slit mask.

The Fresnel mask is based on the properties of the function

$$h(x) = \cos x^2. \tag{2}$$

This function satisfies condition (1) since it can be readily shown that

$$\lim_{L\to\infty} \frac{1}{L}\int_{-L}^{L} \cos x^2 \cos(\xi - x)^2\, dx = \begin{cases} 1 \text{ for } \xi = 0 \\ 0 \text{ for } \xi \neq 0. \end{cases} \tag{3}$$

The practical construction of this mask involves the approximation

$$h(x) = \begin{cases} 1 \text{ for } \cos x^2 > 0 \\ 0 \text{ for } \cos x^2 < 0. \end{cases} \tag{4}$$

This overcomes the difficulty of constructing a mask with spatially varying transmission to X-rays, since only totally opaque or transparent sections are required. In addition to this approximation, realistic masks are of finite length and therefore the condition $L \to \infty$ in equation (3) is not strictly satisfied. It is not therefore surprising that the convolution of such a mask of width $2L$ with a similar mask but of 'infinite' width does not exhibit a single peak but several maxima and minima apart from the main peak.

The wider mask used for reconstructing the source image from the shadowgram will be referred to as the analyser mask.

The ratio F of the transparent area to the total area of the shadowmask is called the relative aperture. Two other parameters related to the mask autocorrelation function are also useful: R, the ratio of the height of the main peak to the mean background plateau height and the full-width at half maximum height (FWHM) of the main peak itself.

The general equation for the Fresnel mask slit coordinates, x, follows from equation (4) by setting $\cos x^2 = 0$ and involves the half width of the central slit (HCS) as an adjustable parameter. Thus

$$x = \text{HCS}\sqrt{n} \text{ for } n = 1, 3, 5, 7, \ldots \tag{5}$$

Mertz, who first employed Fresnel masks for imaging purposes (2) suggested the use of the familiar Fresnel zone plates for the transformation implied by equation (3). Note, however, that although the equation for the Fresnel zone plates is similar to (5), n is allowed to take all integer values, namely 1, 2, 3, 4 . . . . This different definition, although contradictory to equation (4), does not appear to cause any serious deterioration on the form of the convolution pattern, which looks very similar to the patterns obtained with masks based on equation (5), as can be seen from Fig. 1. Furthermore, similar convolution patterns are obtained from masks having their slit coordinates given by the generalized equation $x \propto n^{\beta}$ where $0 < \beta < 1$ and $n = 1, 2, 3 \ldots$ or $n = 1, 3, 5 \ldots$. Examples of such convolution patterns are shown on Fig. 1 together with the relevant parameters. Note that for $\beta = 0{\cdot}5$ the masks become of the Fresnel type, while for $\beta < 0{\cdot}5$ masks with higher F and smaller R are obtained, the opposite being true for masks with $\beta > 0{\cdot}5$, although in this case the changes are marginal.

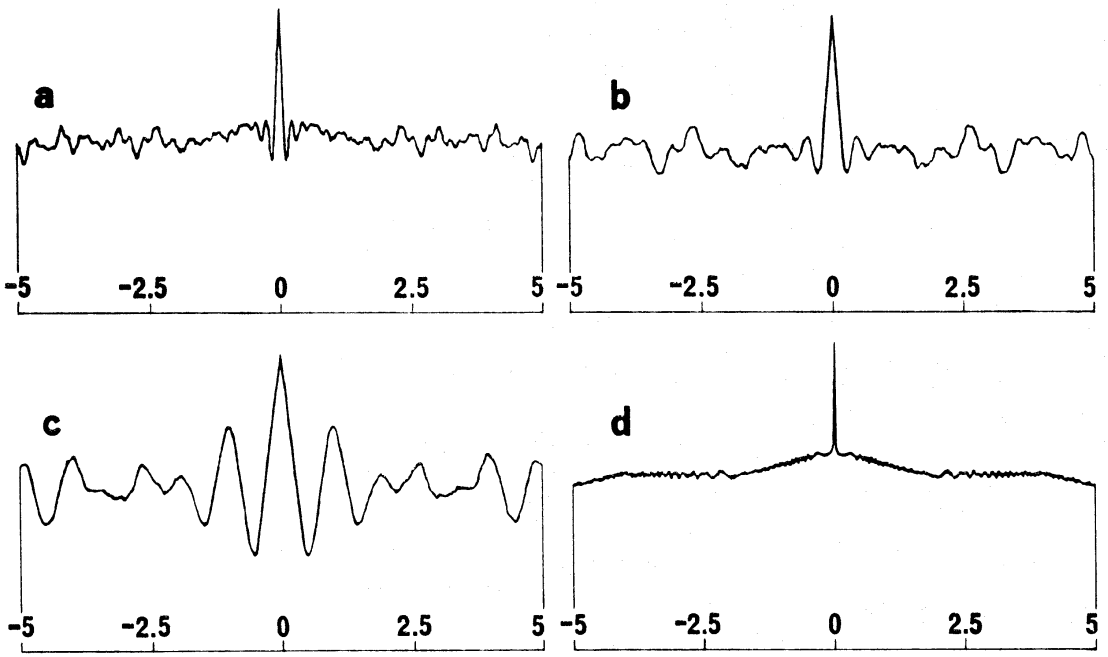

FIG. 1. *Convolution patterns, $I(\xi)$ versus ξ, of various types of generalized one-dimensional masks with the following parameters:* $HCS = 1$, $2L = 10$. (*a*) $\beta = 0{\cdot}5$, $R \approx 1{\cdot}75$, $F = 0{\cdot}581$, $n = 1, 2, 3, \ldots$; (*b*) $\beta = 0{\cdot}5$, $R \approx 1{\cdot}79$, $F = 0{\cdot}565$, $n = 1, 3, 5, \ldots$; (*c*) $\beta = 0{\cdot}75$, $R \approx 1{\cdot}8$, $F = 0{\cdot}565$, $n = 1, 2, 3, \ldots$; (*d*) $\beta = 0{\cdot}25$, $R \approx 1{\cdot}76$, $F = 0{\cdot}588$, $n = 1, 2, 3, \ldots$.

The above remarks are strictly valid only for finite masks having equal resolution capabilities and also having their central sections transparent (slits). If the denomination of transparent and opaque sections is interchanged, than complementary masks are produced having opposite properties to their complements as far as the variation of F and R with β is concerned. With very long masks $(L/HCS \to \infty)$ $F \to 0{\cdot}5$ and $R \to 2$ for any value of β in the range 0–1. The ripples evident in the convolution patterns of masks of the above type near the main peak, greatly reduce the usefulness of such masks for imaging purposes. This serious problem is drastically reduced in two-dimensional imaging, since the ripples in the convolution pattern take the form of concentric rings. For this reason two-dimensional Fresnel masks have been used successfully by Mertz in simulations with visible light (**2**) and attempts at employing them in X-ray observations have been made by Mullard Space Science Laboratory—Willmore (private communication) and Boyd (**3**).

The random slit mask, first suggested by Dicke (**4**) in its two-dimensional form, possesses V parallel slits of equal width s, uniformly and randomly distributed over the range $-L$ to $+L$. Neglecting slit overlap, the parameters F and R are given by

$$F = 1/R = 2L/Vs$$

and the FWHM of the main peak is exactly s.

The random slit mask overcomes the ripple problems associated with the Fresnel masks, but instead suffers from spurious peaks in the autocorrelation function arising from statistical fluctuations. These fluctuations can be reduced by increasing V, keeping F constant. Technical problems in manufacture and computer storage requirements set a practical upper limit to V.

Since the position and magnitude of the spurious peaks in the convolution pattern of a random slit mask depends on the particular random number sequence that was employed for its construction, it is natural to question whether a set of ' random numbers ' exists for which no spurious peaks arise. Such a set would have to be determined by trial and error, a procedure which even with the use of high-speed computers appears to be a formidable task although computerized iterative optimization of sets of random numbers has been attempted by Blake *et al.* (**8**) in an effort to minimize the amplitude of spurious peaks. If, however, the condition of infinite (parent) masks is relaxed then it is possible to construct *periodic* masks that have convolution patterns which are completely free from spurious peaks. The mathematics of the design of such masks, which for obvious reasons will be referred to as ' optimum masks ', is discussed in the following section.

The preceding arguments have been made implicitly for the case of high brightness sources, for which the shadowgram of a point source is an exact replica of the shadowmask. With weak sources photon noise may become important and indeed may predominate over all other sources of image degradation. In these circumstances, if some details of the source to be studied are already known, it may be advantageous to adjust the mask parameters to give the best possible performance for that source. A quantitative discussion of this procedure is deferred until Section 4.

2. THEORETICAL DESIGN CONSIDERATIONS

Consider the class of one-dimensional shadowmasks constructed from N elements of equal (unit) width, each of which is either transparent or opaque. Then such a mask is completely specified by the ordered N-tuple.

$$A = \{\alpha_j : j = 0, 1, 2, \ldots, N-1\} \tag{7}$$

where

$$\alpha j = \begin{cases} 1 \text{ if } j\text{th mask element is transparent} \\ 0 \text{ if } j\text{th mask element is opaque} \end{cases}$$

Such a mask displays optimal performance if the convolution integral $I(\xi)$ of the mask with an analyser mask, obtained by periodic extension of the former, has the form depicted in Fig. 2. This has a single, triangular peak for $\xi = 0$, repeating for $\xi = mN$, $m = \pm 1, \pm 2, \ldots$, against a flat plateau.

This multiplicity of peaks is an inevitable consequence of the periodic nature of the analyser mask. Let k be the number of transparent elements of the mask. Thus

$$k = \sum_{j=0}^{N-1} \alpha_j$$

and the relative aperture, F, will be given by

$$F = k/N. \tag{8}$$

A discrete autocorrelation function, $J(n)$, can be defined for the set A as follows

$$J(n) = \sum_{j=0}^{N-1} \alpha_j \alpha_{n+j}$$

where the addition of subscripts is modulo N.

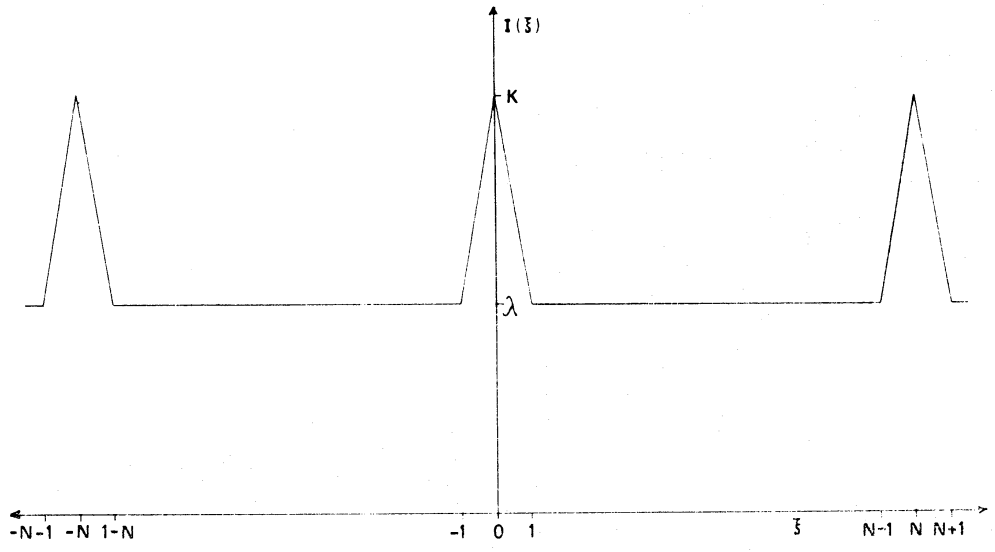

FIG. 2. *Convolution pattern $I(\xi)$ versus ξ, of an optimum mask corresponding to a (N, k, λ) cyclic difference set. The autocorrelation function is identical except that it does not extend beyond $|\xi| = N$.*

The usual autocorrelation function of the mask is clearly the same as the convolution function $I(\xi)$, due to the periodicity of the analyser mask, and can be obtained from $J(n)$ by linear interpolation between the discrete points. The height of the plateau, λ (see Fig. 2), can be found by noting that

$$\sum_{n=0}^{N-1} J(n) = \sum_{n=0}^{N-1} \sum_{j=0}^{N-1} \alpha_j \alpha_{n+j} = \sum_{j=0}^{N-1} \sum_{p-0}^{N-1} \alpha_j \alpha_p = k^2.$$

Thus

$$\lambda = \sum_{n=1}^{N-1} J(n)/(N-1) = (k^2-k)/(N-1). \tag{9}$$

Therefore the peak to plateau ratio, R, is given by:

$$R = k/\lambda = (N-1)/(k-1). \tag{10}$$

Note that for $N \gg 1$, $k \gg 1$, equation (16) becomes

$$R \approx N/k \approx 1/F. \tag{11}$$

The determination of a mask pattern with the postulated properties can be made by exploiting the properties of cyclic difference sets (**5**, **6**). $A\ (N, k, \lambda)$ difference set is a collection of k residues, modulo N, such that for any residue $q \not\equiv 0 \pmod N$ the congruence $d_i - d_j \equiv q \pmod N$ has exactly λ solution pairs (d_i, d_j) with $d_i, d_j \in D$ (i.e. belonging to the set D). The set A defining the mask according to equation (13) can then be constructed according to the rule

$$\alpha_j = \begin{cases} 1 \text{ if } j \in D \\ 0 \text{ if } j \notin D. \end{cases}$$

Examples of the mask patterns obtained by this procedure are shown in Fig. 3, Note that the patterns corresponding to the quadratic difference sets—(*a*) and (*b*)—possess anti-symmetry about their midpoint, if they are extended to the right by one transparent element. This fact can be very useful if the masks are to be con-

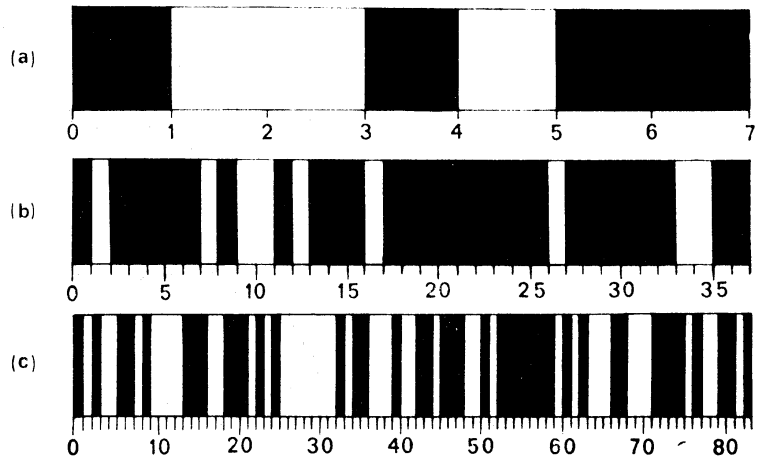

FIG. 3. *Optimum mask patterns with the following parameters:* (*a*) (7, 3, 1) *quadratic difference set,* $F = 0{\cdot}429$, $R = 3$. (*b*) (37, 9, 2) *biquadratic difference set,* $F = 0{\cdot}243$, $R = 4{\cdot}5$. (*c*) (83, 41, 20) *quadratic difference set,* $F = 0{\cdot}494$, $R = 2{\cdot}05$. *Opaque elements are shown shadowed.*

structed photographically since it implies that their photographic negatives are identical to the positives.

It is fairly easy to see that these patterns have the required convolution properties by visualizing one such mask overlaid on top of a similar periodically extended mask. Thus, for $\xi = 0$, $I(0) = k$ since the set D has k elements and therefore the mask possesses k transparent elements (this is not the same as the number of slits since a slit may consist of several consecutive transparent elements, as can be seen in Fig. 3). For any integral value of ξ with $1 \leq \xi \leq N-1$ there are exactly λ solution pairs (d_i, d_j), such that $d_i - d_j \equiv \xi$. Thus $I(\xi) = \lambda$ as required. It can be easily shown that the remaining values are obtained by linear interpolation of these points.

The three parameters of interest in practical applications of optimum masks are: N, determining the resolution of the imaging system, F and R, determining the sensitivity and discrimination of the system respectively. Since F and R are related to each other via equations (8) and (10) only two parameters are required to completely specify a mask.

Baumert (**5**) lists all cyclic difference sets with $k < 100$. For higher values of k tables of difference sets are not available in the literature and therefore one has to generate them.

3. PRACTICAL CONSIDERATIONS

In this section a detailed study is made of the practical considerations in the design of an X-ray telescope system for rocket applications, utilizing one- or two-dimensional optimum masks. The goals of such a design are high sensitivity and resolution coupled with good imaging properties. A schematic telescope set-up is shown in Fig. 4.

The detector is a proportional counter of the type described by Borkowski & Kopp (**7**) which not only provides information about the position of arrival of the X-ray photons, but also their energy. In the one-dimensional case, the resistive wire anodes run perpendicular to the slits, giving the best resolution. Electronic coincidence techniques are used to discriminate against charged particle back-

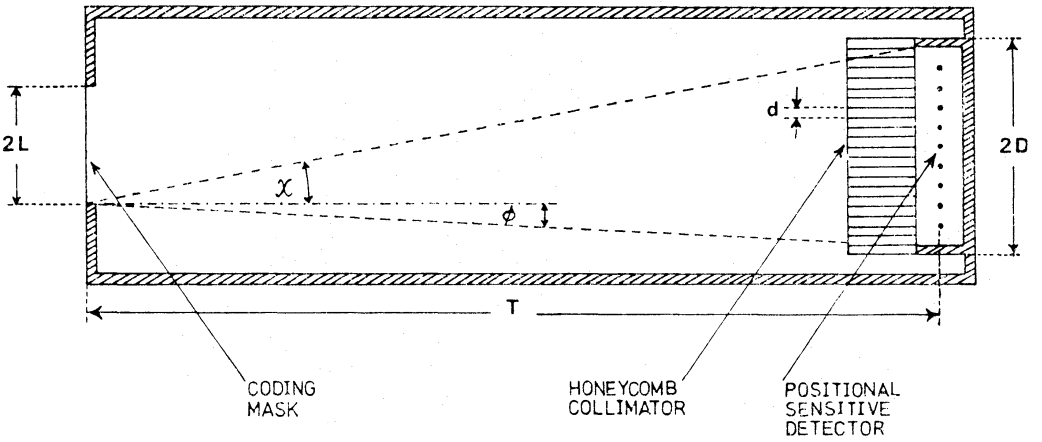

FIG. 4. *Schematic diagram of a proposed rocket-borne X-ray telescope utilizing a coding mask.*

ground, etc. The detector resolution (both perpendicular and parallel to the wires in the two-dimensional case) determines the minimum size of mask element that can be used. For unimpaired functioning of the system the mask element must, in each relevant dimension, be several times the minimum detector resolution.

The honeycomb collimator shown in Fig. 4 is primarily used to support the very thin counter window against expansion as the external pressure falls to zero. It also acts to limit the field of view to avoid ambiguities arising from the periodic nature of the masks and to minimize unwanted counts arising from the diffuse X-ray background (1) and low penetrating power charged particles, e.g. electrons. Unless it is suitably designed, such a collimator can have a detrimental effect on the operation of the overall system, by superimposing further unwanted modulation on the shadowgrams of sources not directly on the telescope axis. To illustrate this, we have computed the effect of a slat collimator, made from thin, parallel, slats of uniform spacing d, on the reconstructed image of a point source. Such a collimator produces a square wave modulation of the shadowgram, with a mark-to-space ratio r, $0 \leq r \leq 1$, depending on the angular distance of the source from the telescope axis. Some results are displayed in Fig. 5.

To avoid these ill effects, we propose to use slat collimators in which the slat spacing is equal to the corresponding width of mask element. (In the two-dimensional case, we have to use such a collimator in each dimension.) In the one-dimensional case, this type of collimator can even be incorporated into the shadow-mask, as illustrated in Fig. 6. Such an ' autocollimating mask ' can be constructed by arranging a slat collimator with thin, parallel slats of uniform spacing s and height τ, the cells corresponding to opaque mask sections being of solid metal.

Assuming for the moment that the thickness of the slats is negligibly small, it is clear that for an *axial* point source the shadowgram obtained with this type of mask will be identical to that obtained with an ordinary mask. If, however, the point source is at an angle θ in the interval $0 < \theta < \psi$, where $\psi = \arctan(s/\tau)$ then the shadowgram projected on the detector is bodily shifted, with respect to the previous case, by an amount $T \tan \theta$, where T is measured from the mask face nearest to the detector. In addition to this shift there is a modification in the form of the shadowgram, since the effective width of the transparent elements is reduced by an amount $\tau \tan \theta$, due to the shadow cast by the slats. The bodily shift clearly does not affect

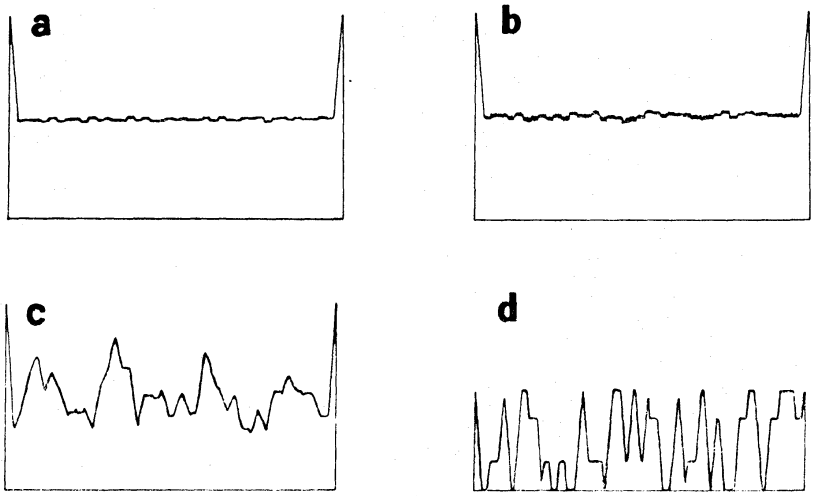

FIG. 5. *Demonstration of the degradation of the reconstructed image of a point source resulting from the use of collimators. A mask corresponding to the* (43, 21, 10) *set was assumed; thus* $F = 0{\cdot}488$ *and* $R = 2{\cdot}1$. (*a*) *Axial source;* $r = 1$. (*b*) *Displaced source, fine collimator;* $r = 0{\cdot}5$, $d = 0{\cdot}286$ *s.* (*c*) *Displaced source, coarse collimator;* $r = 0{\cdot}5$, $d = 10$ *s.* (*d*) *Source near cut-off, coarse collimator;* $r = 0{\cdot}1$, $d = 10$ *s.*

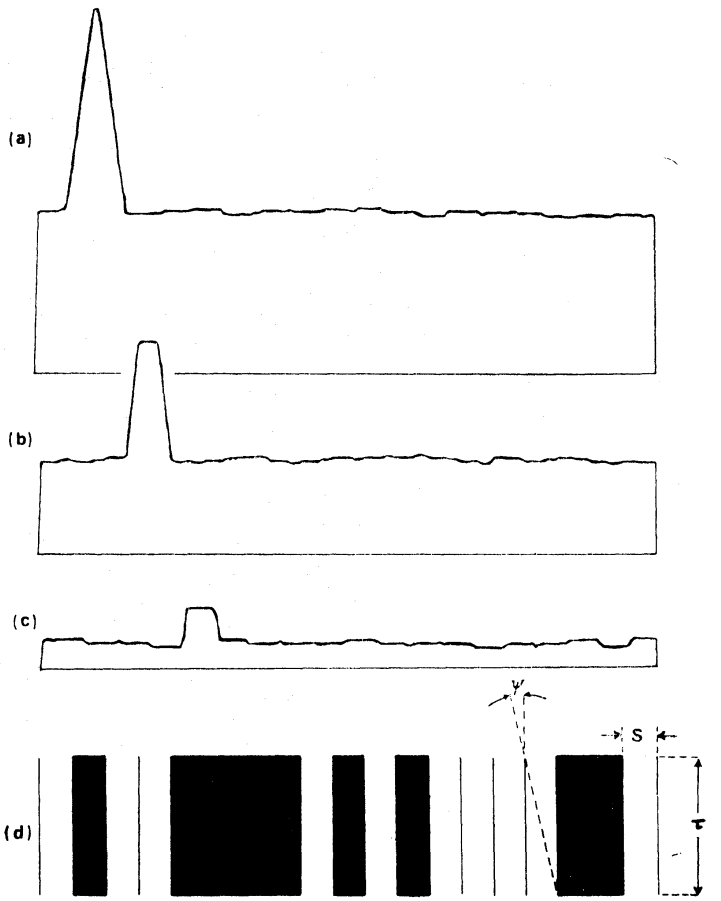

FIG. 6. *Cross-sectional view of an autocollimating, optimum mask corresponding to the* (19, 9, 4) *difference set and the simulated images obtained with it* ((*a*) *to* (*c*)), *assuming a point source at various angles,* θ, *to the telescope axis relative to* ψ. *The parameters are* $F = 0{\cdot}474$, $R = 2{\cdot}25$, $2L = 19$ *and* $s = 1$. (*a*) $\theta/\psi = 0{\cdot}20$, $T/\tau = 10$. (*b*) $\theta/\psi = 0{\cdot}61$, $T/\tau = 4{\cdot}8$. (*c*) $\theta/\psi = 0{\cdot}90$, $T/\tau = 4{\cdot}8$.

the form of the convolution pattern but leads to a displacement of the convolution peak by $T \tan \theta$, this being a feature fundamental to the operation of the telescope. The modification of the shadowgram has the following effects on the convolution pattern which can be seen in Fig. 6.

(a) The peak is truncated as a result of convolving square pulses of different widths.

(b) The absolute magnitude of the whole pattern (neglecting the truncation of the peak) is reduced, due to the effective reduction in the relative aperture of the mask. This is a direct consequence of the collimating properties of the mask. Note that due to the truncation of the peak the value of R (peak-to-plateau ratio) is reduced if the ' peak ' is defined as the value of $I(\xi)$ for $\xi = 0$. A correction can be made for this effect in order to obtain the true (unclipped) value $I_t(0)$ of the peak and hence calculate the intensity of the source either by extrapolating the available sloping edge, or by employing a formula which related $I_t(0)$ and $I(0)$ for any value of θ.

The variation of the plateau intensity with θ, follows the usual triangular response with FWHM $= \psi$ which is characteristic of slat collimators. For $\theta \geq \psi$ no photons are allowed to reach the detector and the shadowgram is blank. Thus the autocollimator mask allows a total FOV equal to $\pm\psi$ and therefore, by making $\psi < \phi$ the possibility of truncated shadowgrams is eliminated. This technique is very appealing since it does not upset the ' optimum ' system response by the introduction of either spurious pulses or noise. The operation of the autocollimating mask can be understood intuitively by visualizing the modified shadowgram as due to a mask having every one of its transparent elements reduced in width by the addition of two opaque strips at its boundary edges. Such an equivalent mask besides its role as a conceptual aid, it has practical application in the construction of rugged, two-dimensional optimum masks, as will be explained in Section 5. The equivalent mask concept also helps in computing the response of autocollimating masks with slats of finite thickness, v. In this case it is clear that the convolution peak will be truncated even for $\theta = 0$. Such a ' thick ' autocollimating mask may be considered equivalent to a thin one (with $v = 0$) but with the source offset by an angle equal to arctan (v/τ).

The autocollimating mask, as described, will restrict the telescope FOV in only one direction. For efficient reduction of unwanted ' events ' due to the diffuse background radiation it is necessary to employ two-dimensional collimation. Although it is possible to achieve this by adding slats in the autocollimating mask in a direction perpendicular to the coding slats it is much simpler to use a separate one-dimensional collimator placed in front of the detector which would also provide the necessary detector window support.

4. NOISE CONSIDERATIONS

With low brightness sources, photon noise becomes the predominant factor determining image quality. By extending the arguments of Dicke (4), we can quantify the effect of photon noise and, in certain cases, find the mask parameters N and F which give the best discrimination against noise for a given set of viewing parameters.

Let t be the exposure time and M be the total number of photons arriving during this time at the shadowmask from all X-ray sources within the FOV and for which

the shadowmask is effective. Let M_0 be defined similarly to M but referring only to the strongest source, and let B refer to the total number of recorded background 'events' that cannot be classed under M. Let Q be the counter efficiency, $\gamma = B/MQ$ and $S = M_0/M$. Assume that these are several point sources in the FOV with different intensities. Thus, in the time interval t a total of $FQM+B$ events are recorded by the detector. After convolution with the analyser mask the reconstructed image will consist of a main peak of height $F(1-F)QM_0$ *above* a plateau of height F^2QM+FB together with further peaks associated with the weaker sources and also random noise.

Since noise crests could be mistaken for source peaks, it is necessary to introduce a measure, η, of the statistical significance of a peak. This is defined as the ratio of that peak height (measured above the mean plateau) for which there is 99 per cent confidence that it does not arise from noise fluctuations, to the main peak height, namely $F(1-F)QM_0$. The value of η can be estimated as follows. For a given element in the plateau of the image, each of the $FQM+B$ counts has a probability F of contributing and $(1-F)$ of not contributing. Taking these probabilities as independent, the probability distribution of the height at this point is binomial with mean F^2QM+FB and variance $F(1-F)(FQM+B)$. For $FQM+B \gg 1$ this distribution may be approximated to a normal distribution with the same mean and variance. Then, for the given element, the probability that there is no peak of height $\eta F(1-F)QM_0$ above the plateau is $1-P(z)$, where

$$z = \eta QM_0\left[\frac{F(1-F)}{FQM}\right]^{1/2} \tag{12}$$

and

$$P(z) = (2\pi)^{-1/2}\int_z^\infty \exp(-x^2/2)\,dx = \tfrac{1}{2}\operatorname{erfc}(z/\sqrt{2}).$$

Although not strictly true, it will be assumed that the probability distributions in each of the n elements of the image are independent. Then the probability that no peak of height $\eta F(1-F)QM_0$ is found anywhere in the image is given by $[1-P(z)]^N \sim 1-NP(z)$ for $NP(z) \ll 1$. Thus for 99 per cent confidence

$$NP(z) = 10^{-2} \tag{13}$$

and z can be found for a given N by numerical solution. The value of z is very weakly dependent on N, e.g. for $10^2 < N < 10^5$, z lies in the range 3·73–5·20. Then η can be obtained from equation (12), namely

$$\eta^2 = \frac{z^2(FQM+B)}{Q^2M_0^2F(1-F)} = \frac{z^2(F+\gamma)}{2M_0SF(1-F)}. \tag{14}$$

If γ is known we can choose F so as to minimize η.

The optimum value of F is

$$F_0 = -\gamma+(\gamma^2+\gamma)^{1/2}. \tag{15}$$

Values of F_0 and η for several typical values of γ and M_0 and for $N = 10^5$ and $Q = S = 1$ are shown on Table I. Values of η^* for $F = 0{\cdot}5$ are also shown for comparison. From this Table it is clear that a low-transparency mask is optimally suited for imaging under low background conditions while a mask with $F \sim 0{\cdot}5$ is best suited for imaging under high background conditions.

TABLE I

Values of η for various values of γ and for two values of $M_0 = 10^3$ (subscript 1) and 10^4 (subscript 2), together with the corresponding values, F_0, of optimized F. Values of η^*, pertaining to the case of constant $F = 0{\cdot}5$, are also shown for comparison.

γ	F_0	η_1	η_1^*	η_2	η_2^*
0·001	0·0306	0·170	0·233	0·054	0·074
0·01	0·0905	0·182	0·235	0·057	0·074
0·1	0·232	0·224	0·255	0·071	0·081
1	0·414	0·397	0·403	0·126	0·127
10	0·488	—	—	0·337	0·337

As an example of the above derivations, consider the case of a single point source with $\gamma = 0$, $Q = 1$ and an optimum mask with $N = 163$ and $F = 0{\cdot}5$. From equations (13) and (14) we find $z = 3{\cdot}85$ and $\eta^2 = 29{\cdot}6/M_0$. Since for positive identification $\eta < 1$, it follows that $M_0 > 30$, i.e. at least 30 photons must arrive at the shadowmask in order to 'image' the course with 99 per cent confidence.

Although the above analysis is valuable in optimizing the telescope design, it does not offer much insight into the actual quality of the images that can be obtained under a given set of conditions, particularly if complex sources are modelled. In such cases it becomes necessary to visually assess actual or simulated

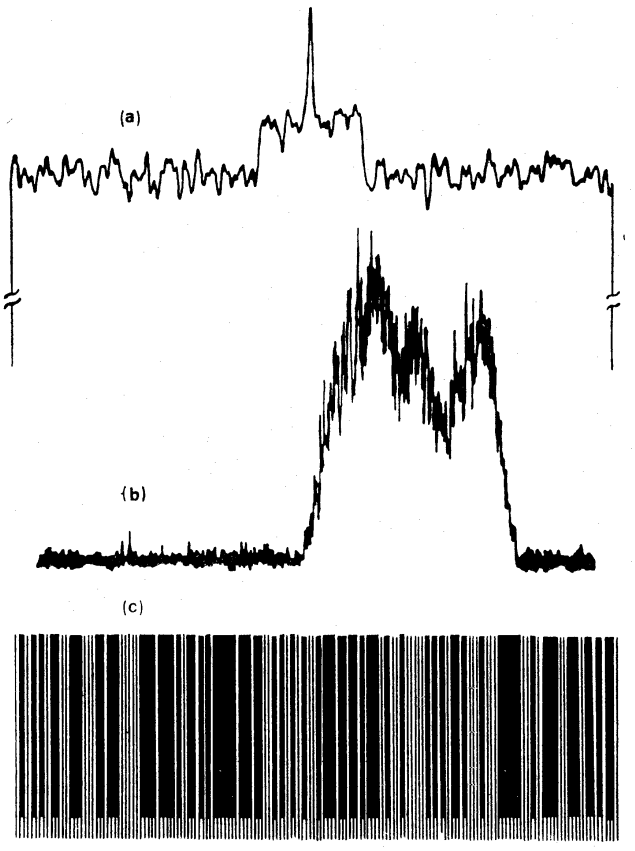

FIG. 7. *Computer simulation of the shadowgram (b) and of the image (a) that would be obtained with an optimum mask telescope pointed at a complex source compounded from point and extended sources as well as background noise. The mask pattern (c), corresponding to the (163, 81, 40) set, is also shown in order to justify the shape of the shadowgram. The source, mask and telescope parameters are given in the text.*

images. An example of such a simulation using a digital computer is shown on Fig. 7. The model assumed for the source, which incidentally formed the basis of a feasibility study for the observation of the X-ray source in the Perseus cluster, comprises a point source located at the centre of an extended source of 45′ angular extent. The ' intensities ' of the point and of the extended source are 3764 and 37 596 photons respectively, i.e. approximately in the ratio 1:10. The extended source is built up from 52 point source of 723 photons intensity each. The simulated shadowgram is assumed to extend over 3 mask periods. A total of 3820 events were randomly distributed over the shadowgram to simulate background events. The assumed mask and telescope parameters are: $N = 163$, $F = 0{\cdot}497$, $2L = 163$ mm, $T = 2{\cdot}19$ m and $2D = 0{\cdot}489$ m. As can be seen from Fig. 7 despite the presence of a bright extended source and considerable background events, both the point and the extended sources are clearly visible. The standard deviation of the noise fluctuations is consistent with the above analysis.

It is clear that, in noisy situations, coded shadowmask telescopes are useful only if the FOV under observation is sparsely populated with a small number of point sources or extended sources with small angular spread. This contrasts with grazing incidence mirrors, whose performance is not degraded by a densely populated FOV.

5. CONCLUSIONS

Under the given constraints of the two-step imaging technique, our class of optimum masks realize the best possible form of mask autocorrelation function. Consequently, where photon noise is not completely dominant, they give a potential increase in performance over the Fresnel and random masks. It is useful to cross-compare the relative advantages of these three classes.

(1) The optimum masks require very careful design of the collimation in order to realize their full performance. One solution, the autocollimating mask, is detailed in Section 3.

(2) Image reconstruction is most conveniently carried out by a digital computer. With high resolution random masks, computer storage requirements for the coordinates of the mask point source function can be prohibitive. Both the Fresnel and optimum masks can use dynamic generation of slit or hole coordinates during run time to avoid this problem.

(3) All the masks have one- and two-dimensional forms. Whereas the two-dimensional Fresnel masks possess radial symmetry, the periodicity of the optimum masks requires them to be based on a rectangular lattice, giving a ' crossword ' appearance.

The mechanical construction of such masks presents obvious difficulties since the structure is generally not self-supporting. The problem can be overcome either by superimposing a high-transparency mesh over the basic mask structure or by decreasing the aperture size of the transparent elements. The latter method results in a truncation of the convolution peak and a uniform height reduction, but does not introduce fluctuations in the plateau (*cf.* the arguments of Section 3).

ACKNOWLEDGMENTS

The authors wish to thank Professor A. P. Willmore for inspiring interest in the theory of coding masks by suggesting the design of a rocket-borne astro-

nomical X-ray telescope utilizing a Fresnel mask, and also for his invaluable advice throughout the development of the project.

They also wish to thank the typists of the University of Birmingham and of BAC Ltd who have greatly contributed in the preparation of this publication.

REFERENCES

(1) Schnopper, H. W. & Delvaille, J. P., 1972. *Sci. Am.*, **227**, 27–37.
(2) Mertz, L., 1965. *Transformations in optics*, John Wiley & Sons, Inc.
(3) Boyd, R. L., 1973. *Q. Jl. R. astr. Soc.*, **14**, 218–233.
(4) Dicke, R. H., 1968. *Astrophys. J.*, **153**, L101–6.
(5) Baumert, L. D., 1971. Cyclic difference sets, *Lecture notes in mathematics*, No. 182, Springer-Verlag.
(6) Storer, T., 1967. *Cyclotomy and difference sets*, Markham, Chicago.
(7) Borkowski, C. J. & Kopp, M. K., 1975. *IEEE Trans. Nuclear Science*, NS17, 340.
(8) Blake, R. L., Burek, A. J., Fenimore, E. & Puetter, R., 1973. *Rev. Sci. Instr.*, **45**, 513–16.